(2)

Center for Night Vision and Electro-Optics

AMSEL-NV-TR-0097

Laser Induced Optical Damage in Solids

by

Gary L. Wood

Edward J. Sharp

July 1991

FORT BELVOIR, VIRGINIA 22060-5677

Destroy this report when it is no longer needed.
Do not return it to the originator.

The citation in this report of trade names of commercially available products does not constitute official endorsement or approval of the use of such products.

REPORT DOCUMENTATION PAGE

Form Approved
OMB No. 0704-0188

1. AGENCY USE ONLY (*Leave blank*)	2. REPORT DATE	3. REPORT TYPE AND DATES COVERED
	July 1991	Final

4. TITLE AND SUBTITLE

Laser Induced Optical Damage in Solids (U)

5. FUNDING NUMBERS

6. AUTHOR(S)

Gary L. Wood and Edward J. Sharp

7. PERFORMING ORGANIZATION NAME(S) AND ADDRESS(ES)

CECOM Center for Night Vision & Electro-Optics (C2NVEO)
Lasers and Photonics Division, Optical Protection & Processing Team
Fort Belvoir, VA 22060-5677

8. PERFORMING ORGANIZATION REPORT NUMBER

AMSEL-NV-TR-0097

9. SPONSORING/MONITORING AGENCY NAME(S) AND ADDRESS(ES)

Same

10. SPONSORING/MONITORING AGENCY REPORT NUMBER

Same

11. SUPPLEMENTARY NOTES

POC: Edward J. Sharp, 703-664-5767

12a. DISTRIBUTION/AVAILABILITY STATEMENT

Approved for public release; distribution unlimited.

12b. DISTRIBUTION CODE

13. ABSTRACT (*Maximum 200 words*)

This report examines some of the many mechanisms that lead to catastrophic damage of solids by high intensity optical radiation. Both surface and bulk damage are explored including: the different mechanisms of avalanche breakdown, thermal breakdown, thermal runaway, acoustic damage, nonlinear effects, the role of plasmas in damage, and the effects of surface preparation on damage thresholds. The relevant radiation and material characteristics are given for each damage mechanism, and the damage thresholds for a variety of materials are reported. Suggestions are offered on ways to raise the threshold for optical damage.

14. SUBJECT TERMS

optical damage, avalanche breakdown, nonlinear effect, plasmas, thermally induced damage, field induced damage

15. NUMBER OF PAGES

37

16. PRICE CODE

17. SECURITY CLASSIFICATION OF REPORT	18. SECURITY CLASSIFICATION OF THIS PAGE	19. SECURITY CLASSIFICATION OF ABSTRACT	20. LIMITATION OF ABSTRACT
Unclassified	Unclassified	Unclassified	

TABLE OF CONTENTS

ACKNOWLEDGMENTS

The authors wish to acknowledge helpful discussions with and suggestions from William W. Clark III, Mary J. Miller, Byong Ahn, and Andrew Mott of C2NVEO, and Gregory J. Salamo from the University of Arkansas.

SECTION I
INTRODUCTION

Optical radiation in our everyday world consists of natural sources such as the sun, scattered sky light, burning objects, etc. Man-made sources include such things as filament lights, fluorescent lights, arc lamps, etc. These incoherent light sources can produce a variety of effects when interacting with matter, but rarely can they cause macroscopic damage (large scale irreversible changes in a material). Some of the highest intensity sources are the mercury lamp, which is capable of intensities around 10^4 W/m^2, and the sun, which upon direct illumination can deliver about 10^3 W/m^2. These intensities can be further increased by focusing with a lens. A 1-inch diameter diffraction limited, f# = 2 lens can amplify a plane wave source 17 million times at focus. However, these sources are not point sources but extended in space and will not focus to Airy discs. As a result, the limiting concentration is given by $(\sin^2\theta)^{-1}$ where 2θ is the full angle subtended by the object.[1]

The sun, which subtends $2\theta = 0.54°$, can be concentrated about 46,000 times. Using nonimaging techniques, the radiation from an extended source can be amplified 56,000 to 80,000 times. For instance, using a combination of lenses and a cone, or mirrors and a cone, these nonimaging techniques can concentrate sunlight to intensities as high as ~10^8 W/m^2, (or 10^4 W/cm^2 as is more often reported when dealing with optical damage intensities). Although these intensities seem high, a typical unfocused pulsed laser can deliver 10^9 W/cm^2. This increased intensity has made extensive new investigations into the interaction of light with matter possible.

This report provides a brief summary of some of the common optical damage mechanisms which exist in solids and that have been reported in the literature. The type of damage considered here is catastrophic or macroscopic and irreversible. Usually the physical damage is observed as a region of the material that is visually different from the surrounding non-irradiated material. This visual difference may be due to material blow-off, cratering, or splatter on surfaces. It may also be caused by chemical changes, fracturing, or a different recrystallization structure after heating the material beyond the melting point.

Optical damage can generally be divided into two categories: thermal and field induced. In highly absorbing materials for incident pulses from cw to ~100 nanoseconds (ns), the dominate mechanism for damage is thermal.[2] In the temporal regime where diffusion is not significant, the important parameter of the radiation is the energy density or fluence, F (J/cm^2), which is the integrated beam intensity over the temporal pulse width. In the temporal regime, where the incident pulse width is much larger than the diffusion time of the material, the important parameter is the peak intensity, I (W/cm^2). For highly transmitting materials (as well as absorbing materials with incident temporal pulse widths less than 100 ns), field effects are the predominate damage mechanism. In this case, the parameter dominating the damage mechanism is the peak intensity. **Figure 1** shows the temporal regions where thermal and field induced damage is most likely to occur for (a) highly transmitting materials, and also for (b) absorbing materials.

Most absorbing materials damage between 1 to 100 J/cm^2, and most transmitting materials damage at intensities from 1 to 100 GW/cm^2. However, transmitting materials may have small absorption centers and absorbing materials can form plasmas at high intensities. As a result, one can generally expect damage to occur in any material if the intensity goes above 1 to 100 GW/cm^2 or the energy density goes above 1 to 100 J/cm^2 (for pulses shorter than the thermal diffusion time).

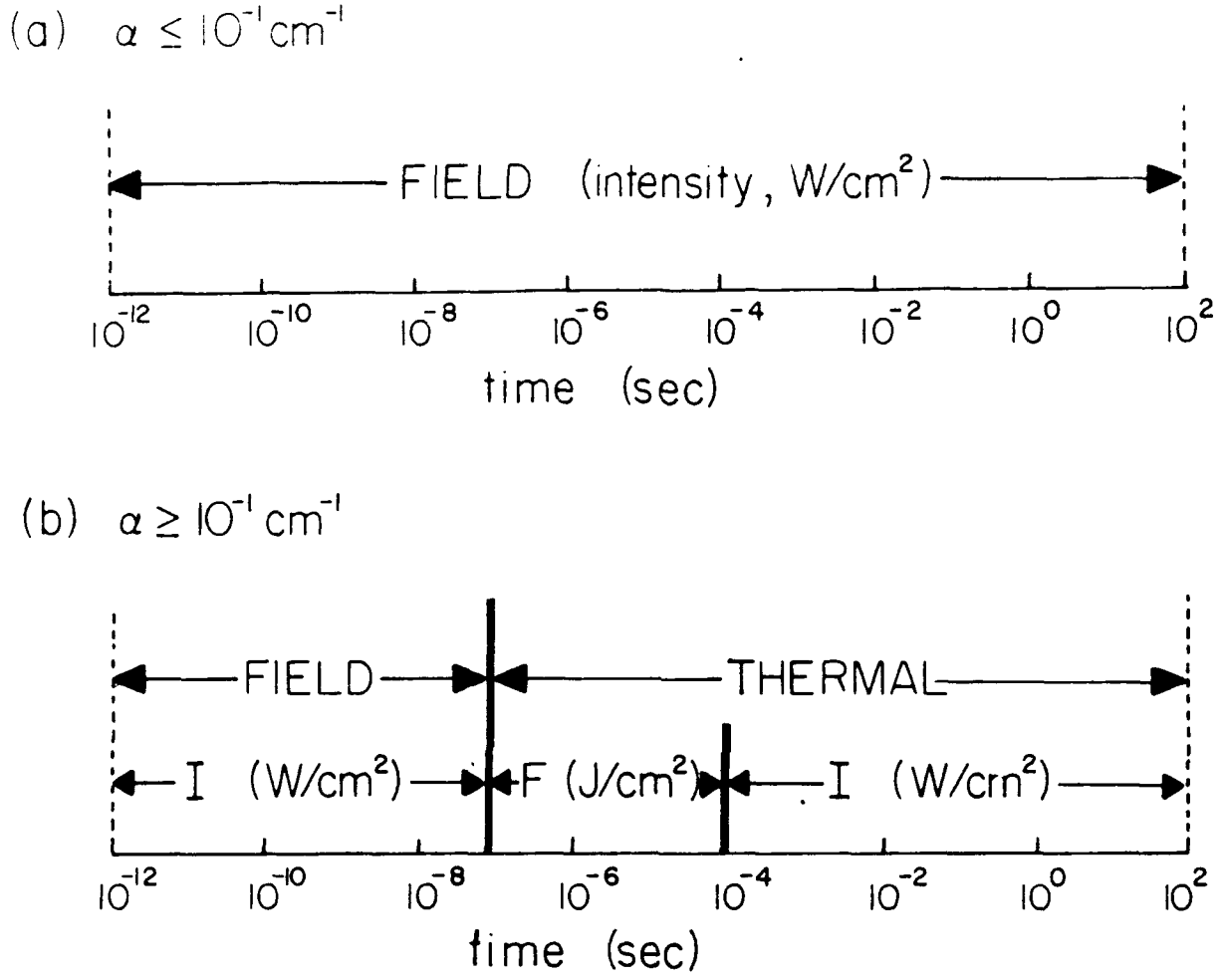

Figure 1. Pulse width regimes for optical damage resulting from thermal and field induced mechanisms.

(a) For highly transmitting materials ($\alpha \leq 10^{-1}\ cm^{-1}$), field effects are the predominate damage mechanism.

(b) For absorbing materials ($\alpha \geq 10^{-1}\ cm^{-1}$), field effects are usually dominant for pulse widths less than 100 nsec and thermal effects usually dominate for pulse widths greater than 100 nsec. In the region where thermal effects dominate, the damage mechanisms change from fluence dependent (J/cm^2) to intensity dependent (W/cm^2), depending on the significance of thermal diffusion.

SECTION II
DAMAGE MEASUREMENTS

Optical damage is easily induced with pulsed lasers. Early studies of laser damage in materials were motivated by damage to laser rods and components.[3] The search for high damage threshold materials was undertaken and continues today. This line of work has proven necessary for the growth and development of lasers as a whole. This effort is still important for laser manufacturers and user groups requiring large energy or high intensity lasers (laser fusion, laser welding, etc). In fact, optical limiters that are designed to protect sensitive optical components and detectors require high damage thresholds in order to perform adequately.[4]

In order to accurately study optical damage to materials, it is extremely important to have a well characterized incident laser beam. The output beam parameters of the lasers used must be well characterized. The temporal and spatial profile, the intensity, the pulse-to-pulse reproducibility, and the frequency must all be known with a high degree of accuracy.

Optical damage values for some typical materials used as optical components are given in the appendices of *Laser Damage in Optical Materials*, by R. M. Wood; Adam Hilger, Boston, 1986. As those tables indicate, there are often orders of magnitude spread in the reported values and often wide disagreement among researchers as to the value of the damage threshold. Some discrepancies can be attributed to differences in the quality of the irradiated samples. The discrepancies often arise because the researchers report thresholds without considering the effects of all the incident beam parameters listed above. Because of the widely differing measurement techniques used, different values of the damage threshold are reported. If the damage mechanism is not known, all parameters of the incident beam become important and merely measuring the intensity, for example, without regard for the spot size is of no value.

In a typical measurement, a single laser beam is focused on a material sample. The focused spot size is noted and the incident energy, as well as temporal pulse width, is recorded so that both the input fluence and intensity are known. Non-transparent samples are visually inspected with a microscope after each pulse or exposure to determine if damage occurred. The pulse energy is then incrementally increased and the onset of damage is recorded. Damage thresholds obtained for single pulse exposures may differ significantly from thresholds obtained by repeated exposures incident on the same spot of the sample. In fact, these two thresholds are obtained from completely independent experiments.

Due to the statistical nature of damage, it is useful to go above the damage threshold (to an energy which produces damage 100% of the time), when irradiating different spots with each pulse. In the transition region, counting the number of times damage occurs per total number of shots gives a probability of damage at that energy. Single position damage measurements must be done a number of times to insure that the particular area irradiated is typical of the material sample being measured.

When measuring transparent materials, the radiation focused into the sample is recollected and focused onto a detector. A microscope is positioned so that the focal volume of the material being irradiated can be inspected after each pulse. This visual inspection is made easier by using a low

power cw laser beam that is co-aligned with the high power irradiating beam. Any increase in scattering of the cw laser beam is an indication that damage has occurred. In addition, any change in the transmission of the sample can be an indication of damage. If the transmission of the sample changes (increases or decreases) with an increase in the incident energy, then it is possible that damage has occurred. If only the high power pulsed beam is being monitored, the transmission of the sample should be remeasured at low energy levels. If it is not the same as before the changes noted at high energies, then some type of damage has occurred, but not necessarily irreversible catastrophic damage. Reversible microscopic changes often occur before irreversible damage. For example, the formation of color centers is often observed in transparent materials before the onset of catastrophic damage. Once these color centers are formed, they can encourage catastrophic damage due to an increase in absorption or stress. It would be advantageous to use these reversible microscopic changes to predict or determine the damage thresholds in a nondestructive manner. There has been some work along these lines[5], but these approaches are not discussed here.

SECTION III
IDEAL MATERIAL

The ideal solid material for resistance to laser damage would be a perfectly homogeneous isotropic solid, with perfectly smooth flat surfaces, and nearly 100% transmission. If this "ideal" material were surrounded by air and irradiated with a normally-incident collimated beam, the rear surface should have a lower damage threshold. The first surface reflects, r, of the incoming electric field and is out of phase with the incident field E_i, therefore the amplitude at the first surface is, $E_1 = E_i(1-r)$. The standing wave reflection at the back surface is in phase; therefore, the amplitude at a half wavelength from the back surface is, $E_2 = t\,E_i(1+r)$. The ratio of the electric fields is, $E_2/E_1 = 2n/(n+1)$, and the intensity at the back surface is greater than the front surface by this ratio squared. The physical mechanism responsible for damage in this ideal material is called dielectric breakdown. Here the material is literally torn apart by the ac electric field. Insulators with large bandgaps may damage in the bulk due to dielectric breakdown. This damage mechanism results in the highest damage thresholds possible. The intensity for dielectric breakdown (db) is given by, $I_{db} = (\varepsilon_0 n c E_{db}^2)/2$ where the electric field is the peak ac dielectric breakdown field given in V/m. It has been found experimentally that the breakdown field is insensitive to the frequency from dc out to 694 nm.[6] Very large bandgap insulators can have $I_{db} > 1000$ GW/cm^2 as a dielectric breakdown intensity. For comparison, clean air has a breakdown intensity on the order of 1 to 1000 GW/cm^2 depending on the wavelength ($I_{db} \propto 1/\lambda$) and the spot size ($I_{db} \propto 1/r_0^2$).[7]

Moving from the "ideal" material into the realm of real materials, a wide range of "imperfections" can cause a material to damage before dielectric breakdown. In addition, the surface of a solid is more sensitive to damage than the bulk because there are more types of imperfections possible on the surface. Section IV outlines many possible physical damage mechanisms that occur in real solids and the imperfections that bring about optical damage.

SECTION IV
DAMAGE MECHANISMS

AVALANCHE BREAKDOWN

Electron avalanche breakdown can occur in all materials and lead to damage. In many laser-hardened transparent materials, this is the mechanism leading to damage; therefore, it is important to investigate this mechanism in more detail than the others. This mechanism is highly nonlinear and very sensitive to the initial spatial and temporal beam profiles. As a result, it is one of the more difficult mechanisms to analyze. It has been the subject of considerable debate in the past and continues to be somewhat controversial. Electron avalanche breakdown can occur in the bulk of the material or on the surface. It involves the generation of a large number of free electrons over a relatively short time. These electrons form a hot plasma that produce permanent changes to the lattice on a macroscopic scale. Electrons in the conduction band are free to absorb incident photons increasing their kinetic energy. At some point, an energetic electron in the conduction band undergoes an inelastic collision with a valence electron and excites it across the bandgap creating an electron-hole pair in the process. Since the electron has a much higher mobility than the hole, the hole can be regarded as stationary and cannot contribute to the generation of the plasma.

Two situations give rise to avalanche breakdown. In the first situation, there are no initial free electrons in the focal volume; in the second situation, there are conduction electrons already present. An estimate of the number density of initial conduction electrons can be found from the conductivity or by knowing the bandgap energy and the Fermi level. The number density is then multiplied by the focal volume to calculate the number of free electrons within the focal volume. In the first situation, an electron can get to the conduction band when irradiated via thermal emission from submicroscopic metal colloids or inclusions, and by tunneling or multiphoton absorption from color centers. These processes are intensity dependent and time is required to form a free electron, unlike the second situation, where electrons are already in the conduction band. Experimentally, these two situations can be distinguished in breakdown experiments. If one observes, as the incident intensity approaches the breakdown field strength, a series of small locally separated damage spots within the focal volume for picosecond pulses, then it is likely there were initially no free electrons.[8] These damaged regions occur where the incoming radiation encountered an easily liberated or initially free electron (for instance, electrons from dopants or defect sites). For longer pulse widths or higher input intensities, these regions will overlap, creating a continuous damage area in the focal volume. On the other hand, for materials with large numbers of free electrons, a continuous damage area in the focal volume is observed even for low input intensities.

Free electrons can be modeled as accelerating under the influence of the incident radiation field until they collide elastically (in some average time) with the lattice (see **Figure 2**). For large angle scattering, the electron effectively remains at the same speed after the collision but changes its direction. The electron then accelerates in the electric field direction and again collides with the lattice but with a larger velocity than in the first collision. The electron is scattered once more at

the new velocity and accelerates as the process is repeated. Eventually, an inelastic collision occurs and an optical phonon is created. The initial electron, having transferred most of its kinetic energy, is left with near-zero velocity. The above process is repeated and the electron again undergoes repeated accelerations from near-zero velocity until another phonon is created. This process will not lead to an avalanche breakdown, but will result in a steady increase in the lattice temperature.

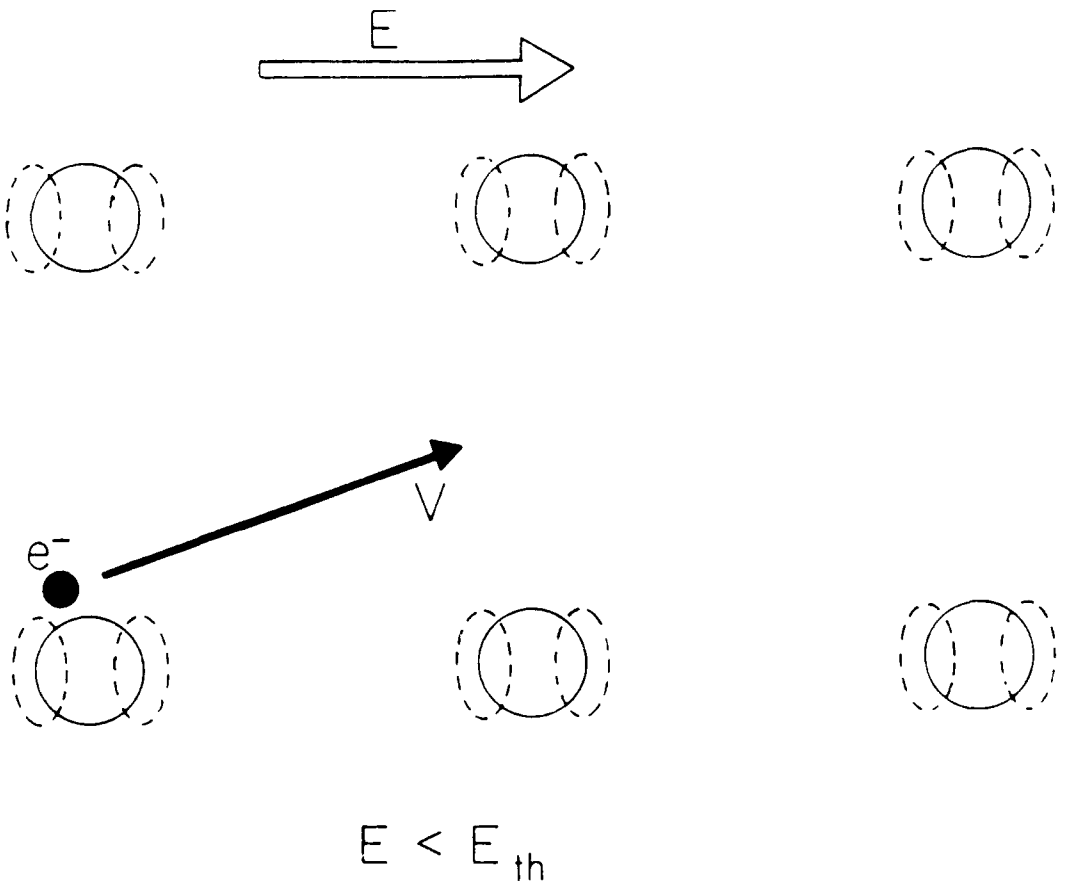

Figure 2. Depicts the situation for a free electron when the optical field is less than the avalanche threshold electric field ($E < E_{th}$). The electron accelerates in the optical field until it undergoes an inelastic collision with the lattice creating a phonon which leaves the free electron with little kinetic energy. This process continues; the electron again accelerates in the optical field, and again collides with the lattice. As a result of these collisions, the heated lattice is shown vibrating about its equilibrium position.

If, however, the electron excites an optical phonon on the first collision with the lattice and has kinetic energy left over, then the electron can continue to gain energy from the incident field. Eventually, the electron will have enough energy to ionize the lattice site and generate a second free electron and a hole as depicted in **Figure 3**.

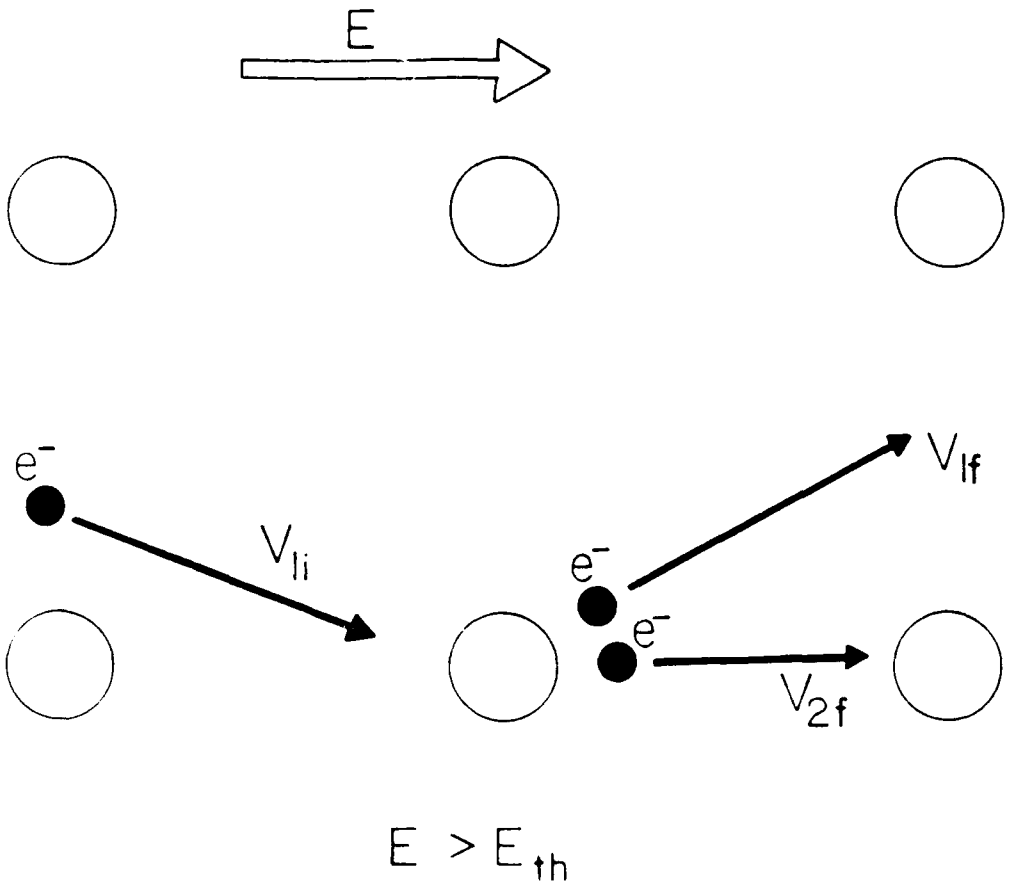

Figure 3. Depicts the situation for a free electron when the optical field is greater than the avalanche threshold electric field ($E > E_{th}$). An electron with initial velocity V1i undergoes an inelastic collision with the lattice and creates a second free electron with velocity V2f. These two electrons then undergo collisions with the lattice resulting in a total of four electrons. This process continues establishing the onset of avalanche breakdown.

As long as the electrons can repeat this process before recombination or diffusion, the process, (e- + photons = 2e- + photons = 4e- + photons = ...) is said to have gain and the generated electrons will eventually form a hot plasma (discussed in Section VI). If the number density of conduction band electrons double every t_I seconds, then,

$$n_c = n_{co} 2^{t_p/t_I} \text{ or } n_c = n_{co} \exp(\omega_c t_p) \quad [1]$$

where n_c is the number density of conduction band electrons, n_{co} is the original number density, t_p is the incident pulse width, t_I is time required to double the density (or the time between ionizations), and ω_c is $0.69^2/t_I$. As can be seen, the conduction band electrons will grow exponentially with time forming a local plasma. The above calculation, however, assumes no losses. Loss mechanisms include the conduction electron recombining or becoming trapped with a hole. Another loss mechanism is diffusion out of the avalanche region. The diffusion distance can be calculated from, $(\tau/3t_I)^{1/2} l_{coll}$, where l_{coll} is the mean collision distance, and τ is the recombination time. Note that all of these losses are negligible for incident pulse widths less than 10 ns.

In order to calculate the incident electric field necessary to generate gain (threshold field), the free electron can be modeled from the force equation as,

$$m d^2x/dt^2 - \gamma dx/dt = eE\exp(i\omega t) \quad [2]$$

where γ is related to the collision rate, m is the effective electron mass, and ω is the frequency of the incident radiation. The average rate of energy gain from the RMS field can be calculated by finding the power, $P = Re(\mathbf{F}\cdot\mathbf{v_d})$, where $\mathbf{F}$ is the electric field force and v_d is the drift velocity calculated from Eq. 2. The total power gain per unit volume is;[6]

$$P_G = e^2E^2\tau_k n_c(t)/m(1+\omega^2\tau_k^2) \quad [3]$$

where the average time between collisions (time constant) for large-angle scattering is, $\tau_k = \gamma/m\omega^2$. The total rate of power loss per unit volume to the lattice is,

$$P_L = n_c(t)\hbar\omega_p/\tau_L \quad [4]$$

where ω_p is the optical phonon frequency, $\hbar$ is $h/2\pi$, and τ_L is the time constant for both large- and small-angle scattering. When the power gained from the incident field equals the power loss due to the generation of an optical phonon, the electric field is the threshold field. Any field larger than the threshold field will allow an electron to gain the energy necessary to ionize the lattice. The threshold field is obtained from, $P_G = P_L$ or

$$E_t = [(m\hbar\omega_p/2\pi e^2)(1+\omega^2\tau_k^2/\tau_k\tau_L)]^{1/2} \quad [5]$$

The time constants, τ_k and τ_L, are on the order of 10^{-15} to 10^{-16} seconds and correspond to the collision frequency of hot (3 - 15 eV) electrons with the lattice.[9] For input fields above threshold ($E > E_t$), an electron will experience energy gain with time and reach the energy (ξ_I, ionization energy) necessary to promote a second electron across the bandgap in a time given by,

$$t_I^{-1} = (\hbar\omega_p/\xi_I\tau_L)([E^2-E_t^2]/E_t^2) \qquad [6]$$

Equation [6] is found by integrating dEnergy/dt = $(P_G - P_L)/n_c$ to get Energy $_0|^{\xi_I} = [p_G - p_I]t_I$ where $p = P/n_c$. When the number density of free electrons reaches a value typically achieved in about 20 to 40 generations, the material will melt.[10] Therefore, the initiation time is related to the pulse width for breakdown by a constant, i.e., $t_p \sim 30t_I$. From Eq. [6], the breakdown field is seen to depend on the pulse width as $E^2 = (t_I^{-1}/C + 1)E_t^2$, where C is some constant, and $t_I^{-1} \sim 30t_p^{-1}$, so $E \propto t_p^{-1/2}$.

Damage is assumed to occur when the lattice temperature reaches the melting point. Actually, the temperature can exceed the melting temperature and the solid becomes superheated. It takes a certain time for the solid to melt and after a site has melted the volume of melted region spreads with velocity v_I.[11] The volume of melted region is given by,

$$V = (2v_I(t_p-t_m))^3 \qquad [7]$$

where t_p is the pulse width and t_m is the time to melt. The velocity v_I is given by,

$$v_I = 2a' f\{1 - \exp[-(H_a(T-T_m))/N_D kTT_m]\}\exp(-G/kT) \qquad [8]$$

where a' is the lattice nearest neighbor distance, f is the Debye frequency, H_a is the enthalpy of melting per unit volume, N_D is the nucleation site density, G is the free energy for atomic diffusion, and T_m is the melting temperature. For times less than the relaxation time, the time to melt is given approximately by,

$$t_m^2 \sim 2\tau/VJ_0 \qquad [9]$$

where J_0 is the static nucleation rate per unit volume given by, $J_0 = N_D f\exp[-(G+G^*)/kT]$, where G^* is the free energy to form a liquid center, and τ is the relaxation rate. The relaxation rate can be written as,

$$\tau \sim [10N_D\mu kTT_m/a'fH_a^2(T-T_m)^2]\exp(G/kT) \qquad [10]$$

where μ is the chemical potential per unit area across the solid-liquid interface.

The temperature of the irradiated lattice can be calculated from $T = \int Pdt/C\rho$, where C is the specific heat, ρ is the density, and P is the power gained by the free electrons from the incident field (Eq. [3]). For an electric field at threshold, the temperature, T, is given as,[7]

$$T = T_0 + (1/C\rho)\int dt\, n_c(t)\{e^2E_t^2\tau_k/[m(1+\omega^2\tau_k^2)]\} \qquad [11]$$

where T_0 is the initial temperature of the lattice, and $n_c(t)$ is the number density of electrons in the conduction band. A general expression for $n_c(t)$ is obtained by solving the following rate equation.

$$d(n_c(t))/dt = \eta(E,t)\, n_c + dn_c/dt|_{tunnel} + \beta E^{2r}/rh\omega - dn_c/dt|_{loss}. \qquad [12]$$

In Eq. [12], $\eta(E)$ is the ionization rate for the cascade process.[8] The second term on the right is the number density created by tunneling. The third term is due to single or multiple-order absorption where r designates the order and β is the appropriate absorption coefficient. The loss terms are due to diffusion of carriers out of the focal volume, recombination, or trapping of the free electrons. The mechanisms which contribute to the number of conduction band electrons are shown schematically in **Figure 4**. As pointed out earlier, the losses are not significant in most materials for pulses shorter than approximately 10 ns. If there are free charge carriers already present in the focal volume, and the electric field is at or above threshold, then the first term on the right side of Eq. [12] dominates and,

$$n_c = n_{co}\exp[\int \eta\{E(t)\}dt]. \qquad [13]$$

If E is assumed to be constant in time (a square pulse), then the integration of Eq. [13] from time $t = 0$ to the breakdown time, t_b, yields the conduction band electron density, $n_c = n_{co}\exp(\eta t_b)$. Substituting this electron density into Eq. [11] gives the breakdown time,

$$\eta C\rho m(T-T_0)\,(1+\omega^2\tau_k^2)/n_{co}e^2E_t^2\tau_k = \exp(\eta t_b)-1. \qquad [14]$$

The breakdown field is proportional to $[1/(\exp(\eta t_b)-1)]^{1/2}$. Notice that in the limit where ηt_b is small compared to 1, the relationship of the breakdown field to the time is the same as found before by calculating the time to produce 20 to 40 generations of conduction band electrons. However, the above calculation shows that damage is reached much faster. This is because the temperature was assumed to raise linearly with the number of electrons in the first model; while here, the temperature is assumed to raise exponentially with the number of conduction band electrons.[6] The time from the generation of the second free electron to the melting of the lattice is very short because the ionization rate η is usually large. Linear absorption in transmitting materials due to defects or dopants effectively looks the same as the free electron process since the electrons are liberated at low intensity levels. If the focal volume initially contains no free electrons, then the incident field can be substantially above the threshold field and yet breakdown would not occur. A multiphoton, excited state process, or tunneling process could, however, generate free electrons.[12] These electrons could come from the valence band or from dopant or defect sites within the bandgap. Since these processes are intensity dependent, it is expected that, near threshold, the initiation of free electrons would not begin until near the maximum intensity or until the middle of the pulse. As was stated earlier, once the free electron is generated and $E > E_t$ then the first term in Eq. [8] for the generation of n_c dominates and breakdown occurs. For two photon absorption, Eq. [12] yields $n_c \propto E^4 t$, and substituting this into Eq. [11] yields a breakdown field proportional to $(t_p^{-1/3})$ if the ionization rate η is very large. Likewise, if the starting electrons are generated from strictly three photon absorption, then the breakdown field is proportional to $t_p^{-1/4}$.

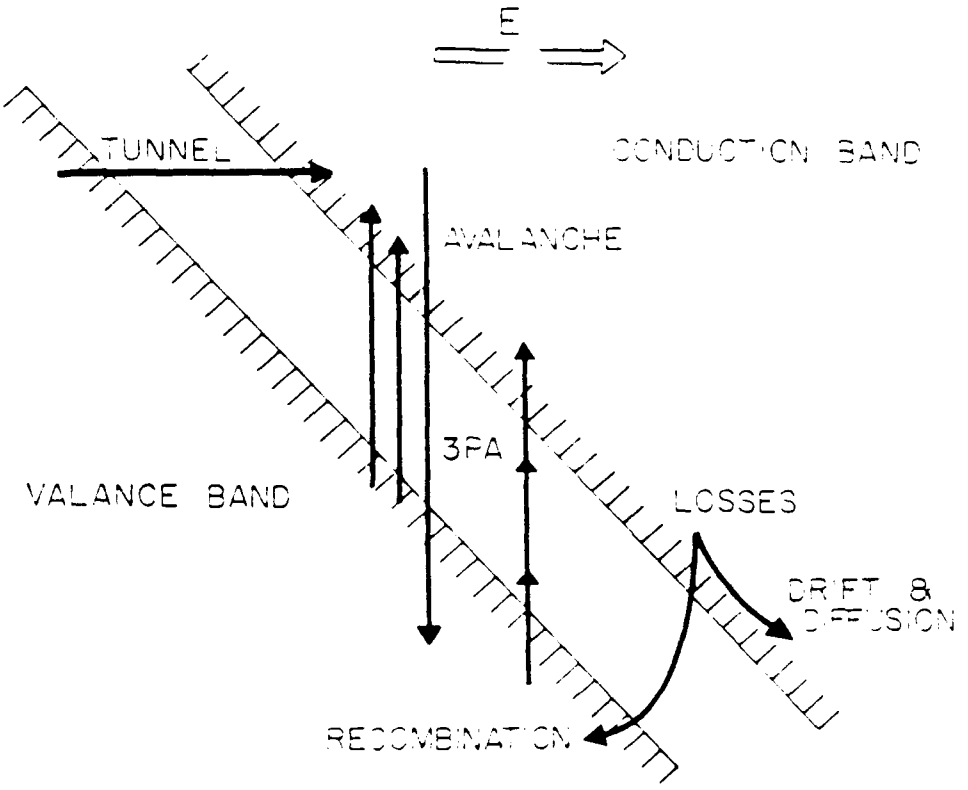

Figure 4. Mechanisms which contribute to the number of conduction band electrons.

AVALANCHE BREAKDOWN (INSULATORS)

In materials with large bandgaps (i.e., the probability of free electrons in the focal volume is much less than 1), the avalanche process is best described by a method proposed by Sparks.[13] The generation of a free electron and the subsequent absorption of sufficient energy to generate a second electron are analyzed here in more detail. Recall that a free electron can be generated either by tunneling (for long wavelength radiation) or through multi-photon absorption (for NIR to UV). A detailed E vs. k graph of the conduction bands for the particular material of interest is necessary. The conduction band electron is now free to absorb the energy of the incident photon and must also absorb a lattice phonon to conserve momentum if a vertical transition will not conserve energy. Additional phonons are absorbed that carry the electron to any value of k with the same E. From these points, the electron is free to absorb an additional photon. This process continues until the electron has enough energy to promote a second valence electron across the energy gap and the entire process is repeated. The conduction electrons increase at a rate according to Eq. [12] and the initiation time (the time it takes the first electron to promote the second electron), t_I, is given by Eq. [6]. Free electrons are energized faster in this model because absorption can occur without the generation of phonons. As noted,[3] the breakdown field is not as frequency dependent from dc out to the visible (red) as predicted by Eq. [5]. However, if the collision frequency were higher, then the theory might agree better but the breakdown field is not accurately predicted. The method by Sparks allows the electrons to energize faster, giving a higher collision frequency, and better agreement with the measured breakdown field.

Avalanche breakdown is a probabilistic event since it involves the random collisions of free electrons to generate other free electrons before recombination. When no free electrons are initially present, avalanche breakdown is still a probabilistic event; however, it is now dominated by multi-photon absorption or tunneling. The probability of forming an inclusion or defect also depends on the history of the material. Upon repeated illumination in the same spot, the probability for damage upon the m^{th} shot can be found from Bass's formula,

$$P_m = (1-P_1)^{m-1}P_1 \qquad [15]$$

where P_1 is the probability of damage on the first shot and is proportional to $P_1 \sim \exp(-k/E)$, where k is a material constant and E is the incident electric field.[14] Perhaps more relevant information is the probability for damage by the m^{th} shot. This is obtained by summing the probabilities given above to obtain,

$$P_{damage} = 1 - (1 - P_1)^m. \qquad [16]$$

It should be pointed out that avalanche breakdown is not the only damage mechanism that is accumulative. Upon repeated illumination, a number of changes can occur—thermo-chemical, migration of dislocations or defects, microscopic defects, or a buildup of particulates on the surface—all of which can be accumulative.

As a result,the probability of damage by the m^{th} shot rises faster than that given by Eq. [16]. However, many materials level off to a near saturation probability after repeated shots. The saturation effect may be due to laser annealing of the surface and defect sites, or to limited microscopic damage which appears to become damage resistant to further illumination.

FREE ELECTRON DAMAGE (NON-AVALANCHE)

There are several breakdown processes which may occur that <u>are not</u> "avalanche" processes since the number of conduction electrons does not continually grow until breakdown occurs. Consider the situation of an incident pulse which is above the electron avalanche threshold for a short time and then falls below threshold before sufficient electrons are generated to melt the lattice. The number of conduction electrons will remain nearly constant (until they begin to recombine, but they can still gain energy from the tail end of the pulse. Sufficient energy may be gained to cause melting and, in this case, the breakdown field would be related to the pulse width as $t_p^{-1/4}$ (if the absorption coefficient depends on I).[15] In fact, if the field produced by the incident pulse always remained below the threshold field, breakdown can still occur when free electrons are encountered, provided enough energy to melt the lattice can be absorbed. Again, the breakdown field would be proportional to $t_p^{-1/4}$. It should be noted that these last two processes are not true avalanche processes since the number of conduction electrons does not continually grow until breakdown. Van Stryland et al.[16] observed that $Eb = A/(t_p^{-1/4}V) + C$ for NaCl and SiO_2 at 1.06 μm in the 40 psec to 31 ns pulse width regime, where A and C are empirical material constants and V is the focal volume proportional to r_0^4/λ where r_0 is the focal spot radius.

In the avalanche breakdown models discussed above, the effects of rising temperature within the irradiated material prior to melting are not considered. The temperature plays an insignificant role in the dynamics of the breakdown process for wide bandgap materials unless the melting point temperature is reached.

THERMAL RUNAWAY

For narrow bandgap materials (semiconductors), the mobility and the number of electrons across the bandgap can appreciably change as the temperature increases. This, in turn, increases the absorption and further increases the temperature. Within a very short time, the material will melt and damage will occur even though the threshold electric field for avalanche breakdown has not been reached. To describe this process, the absorption coefficient must be divided into two parts: absorption due to bound charges and absorption due to free charges. The absorption due to the free charge is dependent on the conductivity which in turn depends on the number density and the mobility. Both the mobility and number density are a function of temperature. The approximate result is,

$$\alpha(t) = \alpha_0 + \alpha_1 \exp[-C/kT(t)] \qquad [17]$$

where α_0 is the bound charge contribution and α_1 and C are material constants. [17] The temperature equation can be written as,

$$dT/dt = \alpha(t)I_0 \exp(-\alpha(t)z)/C_p\rho \quad [18]$$

where C_p is the heat capacity and ρ is the density. This equation describes the thermal runaway process and, as can be seen, is highly nonlinear in temperature. In addition to the rapid change in temperature due to the generation of free carriers, there is also thermal runaway in semiconductors whose bandgap decreases with temperature. As the bandgap decreases,, more charges cross the gap and are able to linearly absorb incident radiation. This also increases the temperature leading to a further decrease in the bandgap, which allows additional free carriers across the gap and so on. ZnSe and ZnS are examples of semiconductors having bandgaps that get smaller as the temperature increases. In addition, the index of refraction increases with intensity for these materials which leads to self-focusing and damage to the bulk (see Nonlinear Effects in Section V).

THERMAL DAMAGE (ABSORPTION)

For a material that is highly absorbing ($\alpha = 10^{-1}$ to 10^5 cm^{-1}) (typical of most detector materials), damage will most likely be due to the localized temperature rising above the melting point at the surface. Bartoli et. al.[2] give an expression for the energy density that produces thermal damage to detector materials. This expression assumes that the incident beams have a Gaussian spatial profile for all pulse widths, σ, and allows for radial diffusion at the surface as well as into the bulk of the material as,

$$F = \Delta T\rho C_p/\alpha(1-R) + (2\pi)^{1/2}\Delta T\rho C_p\kappa\sigma/(1-R)\ \text{atan}^{-1}((8\kappa\sigma/a^2)^{1/2}) \quad [19]$$

where ΔT is the increase in the surface temperature, ρ is the density, a is the beam radius at the *1/e* intensity, σ is a square temporal pulse width for the input intensity, κ is the thermal diffusivity, C_p is the specific heat, and R is the reflectivity. The damage threshold changes from being energy-density (fluence) dependent for short pulses to eventually being intensity (irradiance) dependent at long pulses and out to cw. **Figure 5** shows the measured intensity for the onset of damage vs. pulse width for three typical detector materials (taken from Ref. 2). The agreement between theory and experiment is good. The threshold fluence, F = [J/cm^2], is labeled for each and is constant for adiabatic pulses (short compared to the diffusion time). For pulses where there is enough time for the incident energy to diffuse away during the pulse, the threshold fluence no longer remains constant. When the pulses are long compared to the diffusion time, energy is removed from the irradiated spot through diffusion and, as shown in **Figure 5**, the damage threshold takes on an intensity dependence. In the adiabatic regime, the rise in temperature can be expressed as,

$$T = T_{RT} + (\alpha\, I \exp(-\alpha d)\, \sigma\, (1-R)/C_p\rho) \quad [20]$$

where T_{RT} is room temperature. Since Equation [20] neglects diffusion, it is valid only for temporal pulse widths where $\sigma << (C_p\rho(a/2)^2)/\kappa$. The departure from the short pulse width adiabatic regime has a fluence dependent damage threshold which depends approximately on the square root of the pulse width.[2] As the pulse width is increased toward the cw regime, the damage threshold takes on an intensity dependence.

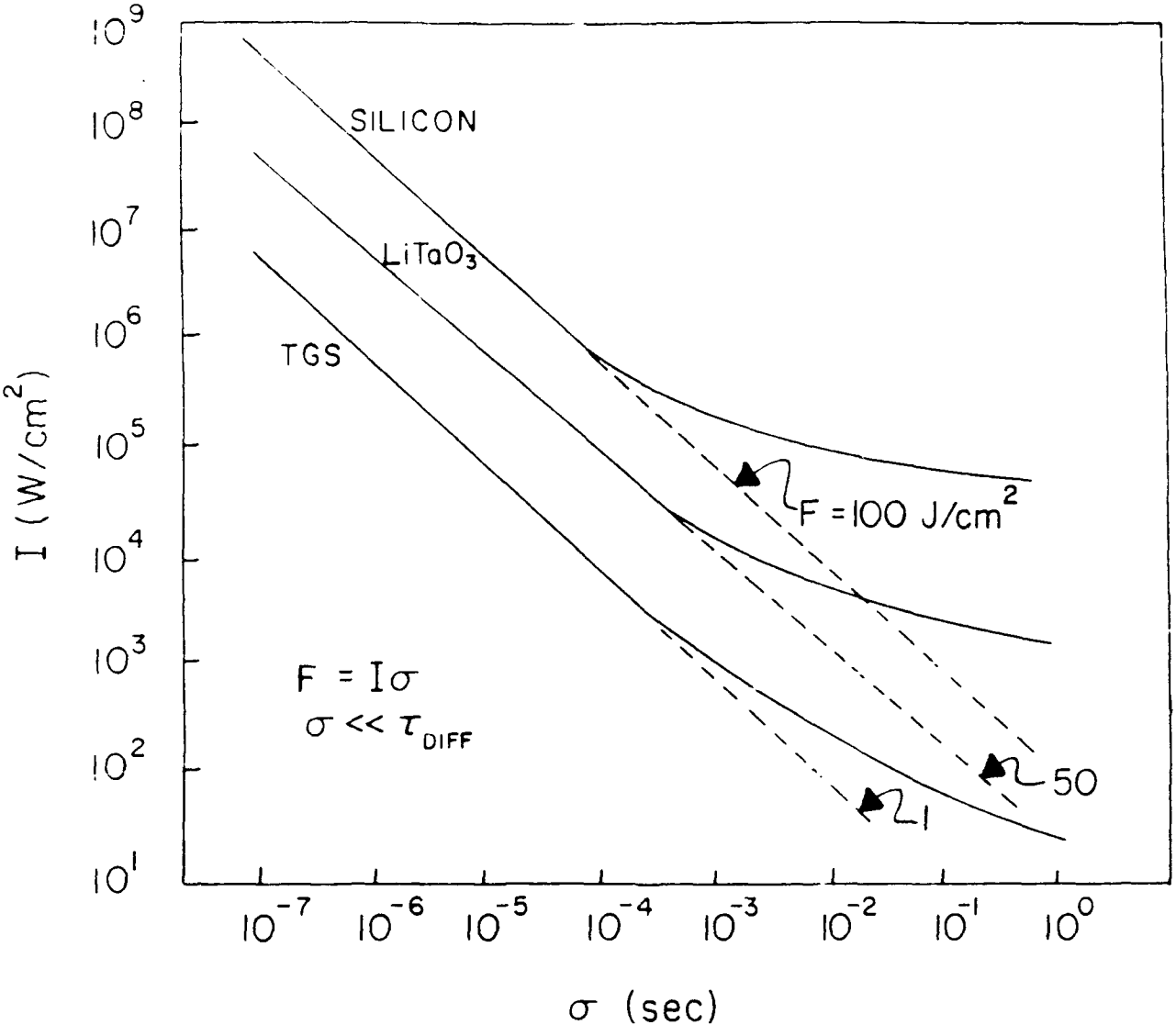

Figure 5. The measured intensity for the onset of laser damage vs. incident pulse width for typical detector materials. This data was collected using 10.6 μm radiation. The deviation from constant fluence, in the pulse width range between 100 μs and 1 ms, is due to the fact that heat is being removed from the irradiated spot through diffusion. This departure from the short pulse width adiabatic regime has a fluence dependent damage threshold which depends approximately on the square root of the pulse width. As the pulse width is increased toward the cw regime, the damage threshold takes on an intensity dependence.

Figure 6 shows the measured damage thresholds of rhesus monkey eyes for energy entering a fixed pupil size vs. laser pulse width for visible and infrared radiation.[18,19] These damage thresholds are compared to the ANSI safety standard (dashed curve) for the human eye. For pulse widths between 0.1 μs and 0.1 ms, the eye is particularly vulnerable to damage. In this pulse width range, the damage depends only on the energy entering the eye; that is, $E \sim 10^{-6}$ I, or for a 1 centimeter aperture (pupil size), this translates into a fluence of 10^{-6} J/cm^2 at the eye. The rise in energy required to produce damage for pulses in the range 1 ns to 0.1 μs is not completely understood but we suggest that it may be due to the formation of a self-protecting plasma.

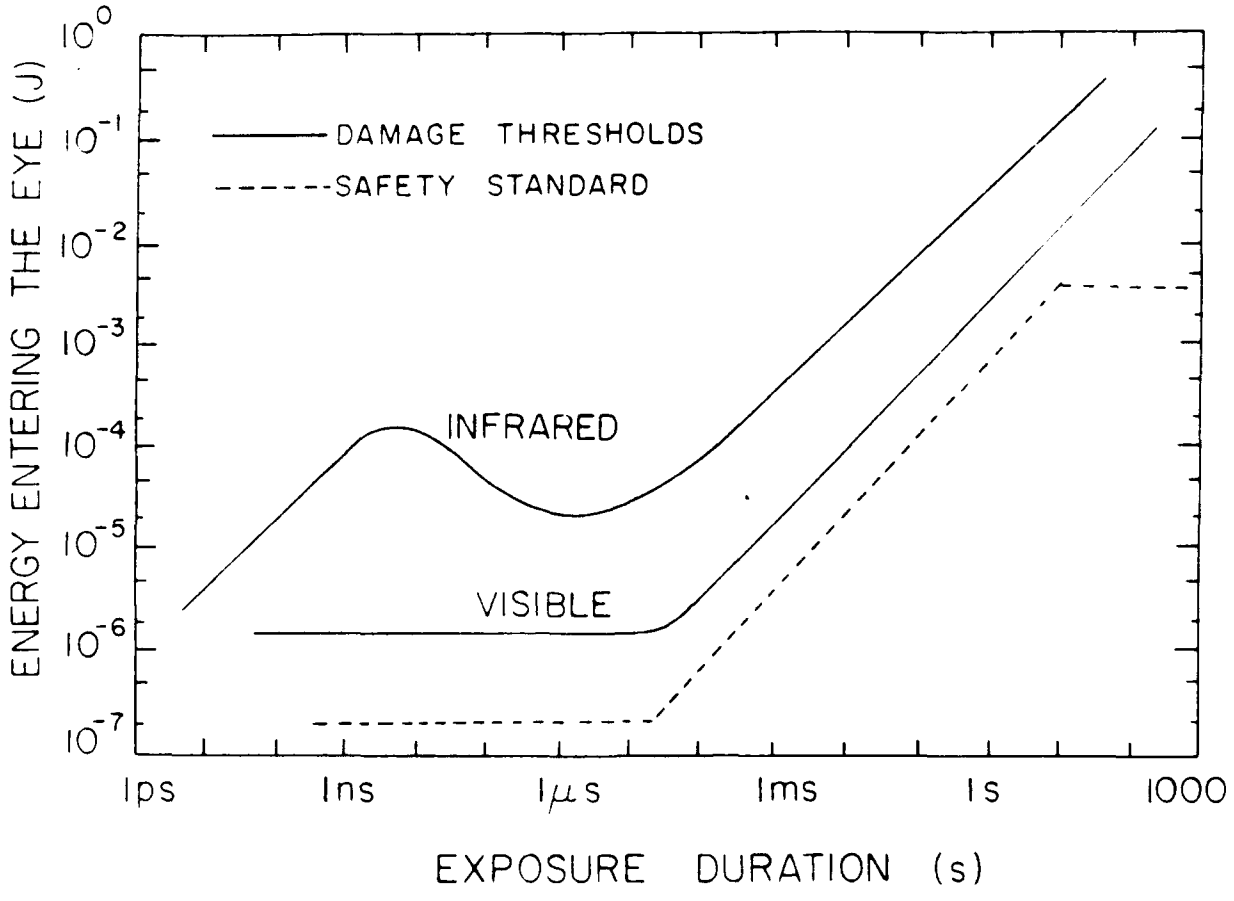

Figure 6. Retinal injury thresholds in the rhesus monkey are plotted as a function of the total laser energy entering the eye vs. exposure duration. The thresholds for both 1064 nm and 532 nm are shown. The dashed curve is the laser safety standard (ANSI Z-136.1).

ACOUSTIC DAMAGE

Stresses formed at the surface of a material or within the bulk can lead to damage.[20] Stresses may be induced from a laser source by absorption and rapid heating, electrostriction, or rapid evaporation. Rapid heating of a localized area may, in and of itself, not cause damage to a medium but the sudden expansion of the heated area may cause so much local stress that the material fractures. Intensity dependent pressure gradients caused by electrostriction can lead to fracture. Rapid evaporation (ablation) at a surface due to high absorption can cause a pressure wave to propagate into the material. Thermo-ionic evaporation at an inhomogenity within the bulk can impart stress within the material as well. In these instances, damage is not caused by melting or chemical changes. In these cases, acoustic waves damage a localized volume by producing cracks or fractures. Stresses induced locally may damage locally but it is also possible for acoustic waves to travel throughout the medium. These waves can travel to the back surface where they may cause damage due to the compression acoustic wave turning into a rarification (tensile) wave upon reflection. One way to distinguish this mechanism from optical mechanisms is to let the radiation be incident on the sample at an angle. Observation of the location of the back surface damage then allows the determination of whether acoustic or optical damage occurs since the two waves will travel at different angles to the back surface within the material. It is also possible for the superposition of waves to enhance the stress on the material. The superposition of rarification waves from an absorbing volume converging at the center of the absorber can create high stresses and lead to damage. If a solid contains a liquid, acoustic waves generated in the liquid may damage the solid/liquid interface especially if the focus is in the liquid. This damage mechanism can easily determined by removal of the liquid.

Stresses may cause microcracks. In addition, micro-cracks may already be present in many materials and acoustic waves will increase the size of these cracks. Transverse phonons with shear stresses could elongate the crack while longitudinal phonons with stresses normal to the crack may open it up more. For a highly absorbing material, a plasma may develop at or before the front surface which generates a shock wave that is imparted to the material propagating across the boundary. The shock wave may cause damage at the front surface or upon reflection from a second surface. The pressure at which damage occurs within the material is called the dynamic fracture stress. It is usually larger than the static fracture stress. Estimates of damage in glass and quartz indicate that the dynamic fracture stress is about 2×10^9 dyn/cm^2 for a pulse width of 1 μs. This value rises an order of magnitude for pulses of about 1 ms. For comparison, 1 atmosphere is 10^6 dyn/cm^2.

The pressure induced by rapid heating due to absorption can be calculated assuming a square temporal pulse.[21] This pulse is subdivided into n parts or t/n time segments. The average temperature at the surface of the absorber after n pulses is,

$$C_v(T_n - T_{n-1}) = F(1-R)/n\rho\delta_{n-1} \qquad [21]$$

where F is the fluence (J/cm^2), R is the reflectivity, T_n is the temperature at n pulses, and δ_{n-1} is the radiation penetration depth after n-1 pulses ($1/\alpha_{n-1}$). Using the energy equation $E_n - E_0 = C_v(T_n - T_0)$ and the Mie-Gruneisen equation of state, $p_n - p_0 = G\rho(E_n - E_0)$, where G is the Gruneisen ratio and E is the energy density per unit mass, the pressure relation is,

$$p_n - p_0 = [GF(1-R)/n] \sum_{i=0}^{n-1} \alpha_i \qquad [22]$$

The α's are temperature dependent and in general decrease as the temperature increases in metals. For example, for radiation at 10 μm wavelength and an intensity of 10^9 W/cm^2 in a 10 ns pulse, the pressure for copper is $p_n = 212 \times 10^9$ dyn/cm^2, and for aluminum, $p_n = 121 \times 10^9$ dyn/cm^2. Before the pressure gets this high, it is likely the intensity will be reduced by plasma absorption and reflection. For nanosecond pulses, the pressure is experimentally found to increase linearly with incident fluences up to about 10 J/cm^2 and the peak pressure for most metals is between 10 to 20 x 10^9 dyn/cm^2. This is an order of magnitude smaller than the predicted values above.

Electrostriction causes stress in transparent materials. The physical mechanism is the distortion of the lattice due to the presence of a strong electric field. Although the incident radiation is an electric field oscillating at high frequency, the lattice sees the average field in time. The electrostrictive pressure is given by,[22]

$$p = (\rho E^2/2)(d\varepsilon/d\rho) \qquad [23]$$

which is about 0.33 atmospheres (0.33 x 10^6 dyn/cm^2) for I = 10^9 W/cm^2 and $\rho d\varepsilon/d\rho$ about 1. This is small compared to the pressures caused by absorption heating and appears to be too small to fracture the material. Much higher electrostrictive pressures can result when the intensity is increased as under self-focusing conditions, for example. In fact, electrostriction is the most likely mechanism for self-focusing of Q-switched ns pulses.[23]

PHOTOCHEMICAL DAMAGE

Some materials may change chemically before melting or fracturing occurs. The heat or absorbed photon energy provided by the laser can increase chemical reactions so that a significant portion of the irradiated surface area changes chemically during illumination. In addition, photodissociation (breaking of molecular bonds) is possible. Most single bonds can be broken with UV radiation at 280 nm. Most single and double bonds can be broken with radiation at 190 nm. A pulsed argon fluoride excimer laser operates at 193 nm and can be used as a precision scalpel, ablating irradiated tissue while not affecting surrounding unirradiated tissue.

SECTION V
MATERIAL DAMAGE

Sections V and VI deal with the problems associated with optical imperfections in highly transparent or "optical materials" such as impurities, irregularities, cracks, or other flaws both on the surface and in the bulk.

SURFACE DAMAGE

The surface is the most susceptible region of a transmitting material to optical damage. Special care must go into producing surfaces which are resistant to high energy laser damage. Any surface irregularities will cause an increase in the surface charge density and hence the local electric field. Surface flatness is not as critical as the condition that the surface be free of all sharp discontinuities. Bloembergen[7] has calculated that the electric field enhancement due to a crack at the surface is, $E_{surface} = n^2 E_{in}$, where n is the index of refraction of the medium containing the crack and E_{in} is the incident electric field. If n is about 3.2, the intensity (which is proportional to E^2) at the surface can be enhanced by a factor of 100. Since it is necessary to have smooth surface features, polishing must be done to high tolerances. Care must be taken to prevent polishing material from being imbedded into the surface. As pointed out earlier these particulates may absorb incoming laser radiation which results in localized surface strain and subsequent damage. Cutting and machining the surface can cause a strain layer up to 10 μm thick. This thin layer may be in a different phase than the bulk and possess a lower damage threshold. Various forms of directed energy[24] have been used to remove a thin (up to 10 μm) surface layer after polishing to improve the laser damage threshold. Mechano-polishing and etching techniques are commonly used to prepare surfaces, but these techniques will not improve a material which possesses low angle grain boundaries and/or grains of soluble material.

Clean surfaces are essential because contaminates can be absorbing or have a low vapor pressure. Surfaces can be contaminated with dust, organic debris, or water amongst other things. In most cases, drying, heating, or washing is sufficient to remove surface contaminants. Materials with low vapor pressure pose a serious problem because the air in front of the surface can breakdown prematurely (i. e., before clean air) and this breakdown causes damage to the surface at lower thresholds. Absorption by a thin surface contaminate layer often occurs with far infrared optics. This thin layer can heat up and cause the bulk material to melt or fracture.

For thin films or thin materials that are well insulated or free standing, heat will primarily be conducted away laterally from the center resulting in a damaged spot which is larger than the input beam spot size. Optical coatings deposited on highly polished transparent materials can often be the cause of lower damage thresholds. For example, dielectric coatings are subject to defects and possibly strain resulting from the thermal mismatch of layers. Evaporation techniques such as RF sputtering, plasma deposition, and molecular-beam epitaxy (MBE) can be used to produce uniform, defect-free coatings. Single crystal MBE films are capable of yielding very high quality films. In those cases where defects are widely scattered over the surface of a material, it is sometimes possible to achieve a higher damage threshold by using a smaller beam spot-size.

OBSERVING SURFACE DAMAGE

Surface damage can be observed directly under the microscope. Because of the rapid cooling that usually takes place, the damaged area has irreversibly changed and the entropy in this area has increased. Single crystals may freeze into polycrystalline forms or become amorphous.[25] Amorphous materials may freeze into polycrystalline or single crystal forms. Nonequilibrium phases can be frozen in by rapid cooling. The stress of rapid heating and cooling causes dislocations to move radially away from the center of focal area. Chemical changes can occur on the surface so that even if the surface recrystallizes into the surrounding surface morphology, it can still be different chemically. This is often easily seen as the damaged area appears darker or lighter than the surrounding medium.[26]

The dynamics of surface damage depend on the material and can be monitored by imaging the reflected radiation. The reflectivity at normal incidence is,

$$R(\lambda,T,t) = [(1 - n^2) + K^2]/[(1 + n^2) + K^2] \qquad [24]$$

where n is the real index of refraction and K is the imaginary index of refraction associated with absorption. Both n and K depend on the wavelength, λ, temperature, T, and the time, t. Slight changes in the reflectivity can be observed when—

—free charges are generated,
—saturation occurs,
—nonlinear effects occur,
—chemical changes occur, and
—the temperature changes.

However, a large characteristic change in reflectivity will always accompany melting. For metals with high conductivites, the melted region cannot propagate far into the bulk of the material. Vaporization, if it occurs at all, is limited for intensities below 10^5 W/cm^2 for 10.6 μm radiation and occurs around the boiling point temperature so that the process is not explosive. Most of the radiation is absorbed within α^{-1} of the surface where the material is in a vapor phase surrounded by a molten layer. For intensities between 10^5 and 10^7 W/cm^2 at 10.6 μm radiation, the surface of a metal will boil and may result in molten droplets being ejected. The explosive ejection of material, which leaves craters on the surface, occurs when $\kappa\alpha\lambda/IC_p$ is small, where κ is the thermal conductivity.[19]

In addition to the above phenomena, a periodic ripple pattern often accompanies surface damage.[27] It is usually observed when the intensity is near the threshold for damage. The ripple grating direction, for normally incident radiation, is in the direction of the dominant electric field polarization. The ripple period is equal to the incident wavelength. For p-polarization, incident off normal, the ripple period varies as, $\lambda/(1 + \sin\varphi)$ where φ is the deviation from the normal to the surface. Ripples are observed for both p- and s-polarized light, but at lower intensities for the p-polarization. Ripple damage is strongly inhibited for circularly polarized light; however, at very high intensities, circularly polarized light will produce a ripple pattern which has randomly oriented gratings. The origin of ripple patterns is closely related to Wood's anomaly. It is believed that a series of scattered waves from surface anomalies interfere with the incident beam. Since

some of the scattered wave running along the surface actually penetrates the surface, energy can be coupled out of the incident beam, across the surface, and into the bulk. The grating that allows this surface scattered wave will be reinforced as the periodically varying energy flux changes the surface through some damage mechanism.

BULK DAMAGE

Inclusions within the bulk can be the source of nucleation centers for optical damage. These localized inhomogeneities may be voids in the lattice, metal or metal-oxide particles, misoriented crystallites, or dielectric-imbedded particles. In some cases, these inclusions may be formed from the incident radiation. Charge carriers and a variety of atomic defects can be produced with varying degrees of mobility. These products may recombine, combine to form new defects or charged states, or become associated with impurities, dislocations, and other defects. Absorption by the inclusion can create a stress fracture. Extreme local heating and the accompanying mismatch of thermal expansion between the inclusion and the surrounding material causes irreversible strain. Damage may also occur when the material surrounding the inclusion melts. It can be determined if the damage was caused by inclusions if, when viewed through a microscope, the damaged spot is observed to be located outside the focal volume. Damage caused by stress depends on the inclusion size. For visible and near infrared radiation, the intensity to produce damage is inversely proportional to the inclusion size for small inclusions (0.1 μm). For intermediate size inclusions (1 μm), absorption occurs only within the inclusion and the expansion of the inclusion causes damage. In this case, the energy density to cause damage is proportional to the inclusion size. For large inclusions (>9 μm), only the surface of the inclusion expands. The energy density required to produce a stress fracture is proportional to the square root of the pulse width. Thermal damage caused by inclusions can be found from the following formula,[28]

$$F_c = 4\pi T_c a \kappa_h t_1 / Q(1-(\pi D_h t_1)^{1/2}) \qquad [25]$$

where t_1 is the pulse width, a is the inclusion size, F_c is the energy density at which damage occurs, κ_h is the thermal conductivity of the host, D_h is the thermal diffusivity of the host, T_c is the critical temperature, and Q is the absorption cross section. Often, the damage associated with the inclusion extends beyond the inclusion diameter.

As pointed out in Section IV, any free electrons within the bulk can lead to damage by way of avalanche breakdown, thermal breakdown, or thermal runaway. Free electrons are rare in good insulators; however, the probability of encountering free electrons increases as the spot size within the bulk is enlarged. Impurities or defects (as shallow traps) within insulators also may yield free electrons more readily. Even a good optical quality crystal can have numerous such sites for free electron generation. For example, F-center concentrations as large as 10^{12} are difficult to detect by conventional absorption spectroscopy in alkali-halide samples.[6] Thermal-ionic emission from microscopic inclusions is another possible source of free electrons. If free electrons are not initially present in the irradiated volume, they can get to the conduction band by tunnelling or by multi-photon absorption. This can also happen at susceptible sites as described above. These effects can be sorted out since they require high intensity and the initiation of damage is likely to occur near the peak of the incident pulse. In addition, damage is likely to occur within the focal volume or the most intense portion of the beam.

Organic materials have been reported with very large damage thresholds. Garito reports[29] that diacetylene polymer crystals have a damage threshold of 1 GW/cm^2 (25 ns) and Flytzanis[30] reported PTS polydiacetylene to have a threshold of 10 GW/cm^2 (picosecond pulses). The exact damage mechanism (or sequence of events leading to damage) is inconclusive for PMMA.[31] For example, single-shot damage is either caused by inclusions or by microstructure defects, and multiple-shot damage is related to the viscoelastic properties of the material.[32] Typically, polymer materials sustain multiple-shot damage in the bulk due to carbonizing (soot products formed from polymer breakdown) in areas of microdamage (<10 μm). Exactly in the pulse sequence when the carbonization takes place is the subject of debate.[33, 34] However, once these spots develop, they absorb more radiation and grow until melting or cracking occurs.

NONLINEAR EFFECTS

In transparent materials, optical nonlinearities play an important role in the creation, dynamics, and understanding of optical damage. Self-focusing is possible in any material with a positive nonlinear index of refraction ($n_2 > 0$). The nonlinear index is defined as, $\Delta n = n_2 |E|^2/2$. When the incident power reaches some critical level, the beam collapses on itself resulting in a dramatic increase in the local intensity. If the material is "optically thick" (i.e., the thickness is greater than the Rayleigh range, $z_0 = \pi r_0^2 n/\lambda$, where r_0 is the beam radius), then beam collapse can occur within the material and the high intensities generated by the decreasing spot size will cause the generation of free carriers and a plasma. The second critical power ($P_{cr} = 3.77\, c\varepsilon_0\lambda^2/8\pi n_2$ in mks units and n_2 is in esu units) gives the correct threshold power for Gaussian beams.[35] The effects of self-focusing on laser-induced breakdown were studied in fused quartz and NaCl by Williams et. al.[36] They determined for both materials that self-focusing dominates the damage breakdown process when the power approached the second critical power, P_{cr}. The most likely mechanism for the nonlinear index in these materials for ns excitation is electrostriction.

Irradiating a material at an incident power greater than critical power for self-focusing does not always guarantee that self-focusing will occur. For example, the generation of free carriers reduces the index of refraction with intensity.[37] Generally, the free carrier contribution or Drude contribution to the index of refraction is negative and serves to defocus the beam. In other words, if the Drude contribution to n_2 becomes dominant, then the extremely high intensities associated with self-focusing may not occur. However, it can be argued that, in most cases, the self-defocusing caused by the generation of free carriers occurs after the plasma temperature is above the melting temperature.

Another nonlinear optical phenomena often associated with damage is stimulated Brillioun scattering (SBS)[38] which is due to the scattering of radiation from self-generated pressure waves. SBS occurs above some critical threshold intensity and the acoustic pressure waves created by the incident pump light may become intense enough to cause damage within the material.

SECTION VI
PLASMAS

Plasmas are often created on the surface or in the bulk of a solid by optical radiation[39] and are typically characterized by a plasma frequency. For plasmas in solids, the dielectric constant can be written as,[40]

$$\varepsilon(\omega)/\varepsilon_0 = 1 - \omega_p^2/\omega^2 + \varepsilon_b/\varepsilon_0 \qquad [26]$$

where ω_p is the plasma frequency given by, $\omega^2_{plasma} = n_c e^2/\varepsilon_0 m$, n_c is the free electron density, and ε_b is the background lattice dielectric constant which is a function of n_c.

When $\omega = \omega_p$, $\varepsilon(\omega_p) = 0$, and since $D = \varepsilon E = \varepsilon_0 E + P$, then $\varepsilon_0 E = -P$. This shows that the electron gas field tries to cancel out the incident field creating a longitudinal oscillation. If the irradiating beam is generating free electrons, the electron number increases and the plasma frequency can become greater than the incident frequency. Since $\varepsilon/\varepsilon_0 = n^2$, and ε becomes negative when $\omega_p^2/\omega^2 = n_b^2$, the index of refraction becomes purely imaginary, $n = iK$, and the electron gas can no longer support a propagating wave, i.e., $\exp(ik_0 nz) \rightarrow \exp(-k_0 Kz)$. Instead, the radiation is reflected and the plasma density is maintained at $\omega_p = n_b\omega$ in the steady state.

As discussed earlier in Section IV, a plasma is formed when free electrons are accelerated under the influence of a radiation field and participate in inelastic ionizing collisions with the lattice. As the number density of ions increases, the absorption is increased due to the extra free ion absorption. When the absorption coefficient gets to be on the order of the confocal beam length, rapid heating occurs in the focal region. The material locally melts, forms a plasma and, as time goes on, becomes almost completely ionized. The temperature within the plasma is fairly uniform as the electron diffusion length is on the order of the plasma size. Some energy is lost in blackbody radiation but the amount lost is small compared to the incident energy. Energy that goes into producing the plasma and energy which interacts with the plasma serves to reduce the incoming radiation (usually from the peak intensity and after). This limits the production of free electrons and the transmission through the material. Of course, if the plasma frequency is reached, this dramatically limits the transmitted radiation and freezes the production of electrons.

The high temperature associated with the production of free electrons in the avalanche process creates a high pressure within the focal region and the plasma rapidly expands. Thermal energy goes into the kinetic energy of radial expansion. The radial expansion may be accompanied by a decrease in ion density which depends on the degree of ionization with temperature and time. Any decrease in the plasma density reduces the absorption and concomitantly reduces the temperature. Transmission is again restored and the plasma will lose energy predominantly through bremsstrahlung. The plasma can be formed on the picosecond time scale (> 6 psec) once a free electron is generated.[41, 15] However, for picosecond pulses, the plasma density is significantly reduced and the material will begin to transmit again before the pulse is over. This is not the case for nanosecond and longer pulses where the longer term high plasma density effectively limits the transmission of the input beam. **Figure 7** shows the temporal evolution of the transmitted intensity for the two time regimes.

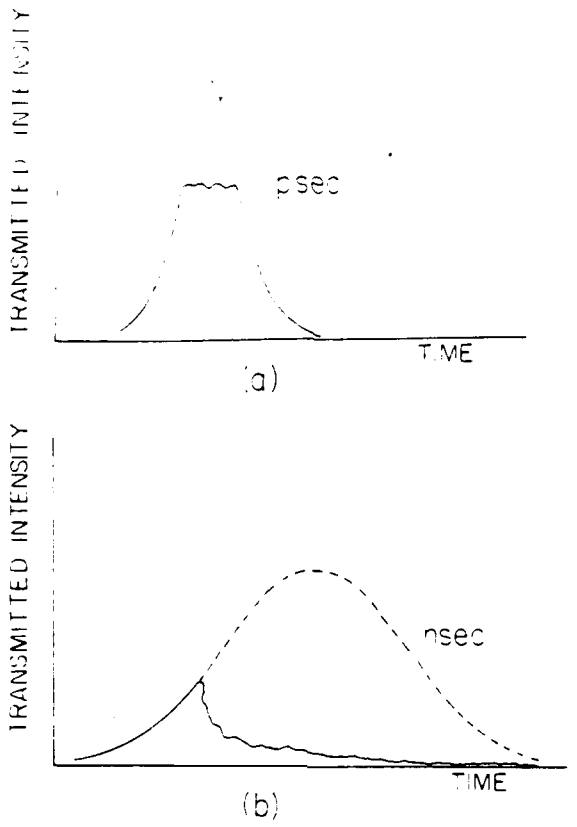

Figure 7. The temporal evolution of the transmitted intensity for plasmas formed by (a) picosecond pulses and by (b) nanosecond pulses.

As mentioned earlier, the breakdown threshold for air can be lower than some materials. This may serve to protect the material from damage in some cases. If the plasma is in air near a surface, blowoff material from the surface will create free charges, vapor, and aerosols that break the air down at even lower intensities thus providing some protection to the surface from the remaining radiation.[42] However, for repeated irradiation, charges build up on the surface and damage occurs. Surface melting may occur when the heat generated by a nearby plasma conducts onto the surface. A lowering of the damage threshold can occur when short wavelength radiation generated by the air plasma is strongly absorbed by the surface. This effect is known as enhanced coupling and has been observed for pulsed as well as cw radiation.[43]

Once a plasma is generated, it fills the focal volume of the laser beam and may even extend beyond it. The plasma will propagate back toward the source because the intensity of the beam will be higher in that direction than in the forward direction. The temperature of the plasma can be very high (tens of thousands of degrees Kelvin). The shock wave associated with a rapidly expanding plasma can produce damage to the surrounding medium. This shock wave is, in fact, easily detected with a transducer and can give a better indication of breakdown than the visible flash of the plasma.[44]

SECTION VII
HOW TO AVOID DAMAGE

Accurate damage measurements are extremely important because damage thresholds for specific optical components often set the upper bound for the radiation levels that many sophisticated optical systems (both imaging and non-imaging) can withstand. Implementing ways to raise the damage threshold of these systems requires an understanding of the damage mechanisms. We have reviewed these mechanisms in the preceding sections.

We now propose a brief summary of methods or techniques to increase the damage threshold of materials by simply avoiding conditions which make the possibility of damage more likely to occur. All optical components exposed to high radiation levels must have well cleaned surfaces. The surfaces should be smooth and crack-free. No polishing material should be imbedded within the surface and there should be no strain on the surface layer. The material should be defect- and inclusion-free with a minimum of grain boundaries. The lattice of any crystalline components should be as closely packed as possible to discourage impurities. By rapidly cooling some materials, it was possible to inhibit precipitation of clusters of impurities which act to lower the damage threshold.[45] If possible and the system or application permits, the incident radiation should be circularly polarized. The material of choice should have the widest bandgap and the highest melting point temperature of the materials available. The change in index of refraction of all surface coatings should be minimized. All optical coatings should have the same thermal expansion coefficients as the bulk material. The focal volume should be made small to minimize the possibility of encountering a free electron in insulators. If possible, irradiation should not occur repeatedly in one spot. All components should be able to efficiently conduct heat away. For instance, diamond-coated optics have a higher damage threshold because of the large thermal conductivity of diamond. The material should be as thick as possible when focusing within the bulk of the material. In addition to all of the above, the material should have a negative nonlinear index of refraction to discourage self-focusing, unless the material is thinner than the Rayleigh range. It is not possible to follow all of these suggestions simultaneously as many involve trade-offs in performance, cost, complexity, and implementation issues. However, higher damage thresholds can certainly be achieved if these trade-offs are made wisely.

SECTION VIII
SUMMARY

In summary, we have reviewed optical damage mechanisms and have discussed ways to isolate and determine the thresholds for damage. We have indicated that optical damage can arise from many possible physical mechanisms and that each has a characteristic behavior which can be used to identify it. The required optical measurements to accomplish this task need to be performed with care and, in all cases, the incident beam must be well characterized.

The properties of an "ideal" material are contrasted with those of a real material and the damage mechanisms associated with real materials are reviewed. Included in the review are:

- avalanche breakdown,
- avalanche breakdown in insulators,
- thermal breakdown,
- thermal runaway,
- thermal damage due to absorption, and
- acoustic damage.

Issues associated with obtaining good transparent optical materials are addressed with emphasis placed on reducing surface and bulk damage. The effects of nonlinear interactions and the role of plasma formation in the damage process are reviewed. Finally, a few possibilities for reducing the probability of optical damage are suggested.

REFERENCES

1. P. Gleckman, J. O'Gallagher, and R. Winston, "Approaching the Irradiance of the Sun Through Nonimaging Optics," *Optics News* **15**:33, May 1989.

2. F. Bartoli, L. Esterowitz, M. Kruer, R. Allen, "Irreversible Laser Damage in IR Detector Materials," Appl. Opt., **16**:2934 (1977).

3. A. J. Glass and A. H. Guenther, eds., Damage in Laser Glass, ASTM Special Technical Publication 469 (ASTM, Philadelphia, 1969).

4. G. L. Wood, "Optical Damage and Optical Limiter Design," Proc. of the 27th IRIS Symp. on IRCM, 1989.

5. S. E. Clark and E. C. Emmony, "The Early Detection of Laser-Induced Damage," IOP Publishing Ltd., p. 466, 1989.

6. D. W. Fradin, E. Yablonovitch, M. Bass, Appl. Opt., **12**:700 (1973).

7. P. Woskoboinikow, W. J. Mulligan, H. C. Praddaude, D. R. Cohn, Appl. Phys. Lett., **32**:527 (1978).

8. W. L. Smith, "Laser-Induced Breakdown in Optical Materials," Opt. Eng., **17**:489 (1978).

9. N. Bloembergen, "Laser-Induced Electric Breakdown in Solids," IEEE J. Quantum Electron., **QE-10**:375 (1974).

10. F. Seitz, Phys. Rev., **76**:1376 (1949).

11 O. Bostanjoglo and E. Endruschat, Phys. Status Solidi A, **91**:17 (1985).

12. P. Braunlich, A. Schmid, "Contributions of Multiphoton Absorption to Laser-Induced Intrinsic Damage in NaCl," Appl. Phys. Lett., **26**:150 (1975).

13. M. Sparks, "Current Status of Electron-Avalanche-Breakdown Theories," *NBS Special Publication 435*, U.S. Government Printing Office, pp. 331-346, 1975.

14. M. Bass and H. H. Barrett, *NBS Special Publication 356*, p. 76, 1971.

15. J. R. Bettis, R. A. House II, and A. H. Guenther, "Spot Size and Pulse Duration Dependence of Laser-Induced Damage," *NBS Special Publication 462*, p. 338, 1976.

16. E. W. Van Stryland, M. J. Soileau, A. L. Smirl, W. E. Williams, "Pulse-Width and Focal-Volume Dependence of Laser-Induced Breakdown," Phys. Rev. B, **23**:2144 (1981).

17. D. L. Mitchell, P. C. Taylor, S. G. Bishop, Solid State Commun., 9:1833 (1971).

18. D. H. Sliney, "Interaction Mechanisms of Laser Radiation with Ocular Tissue," in *Laser Induced Damage in Optical Materials: 1982*, eds. H. E. Bennett, A. E. Guenther, D. Milam, and B. E. Newnam, *NBS Special Publication 669*, January 1984.

19. D. Sliney and M. Wolbarsht, *Safety with Lasers and Other Optical Sources*, Plenum Press, New York, 1985.

20. J. F. Ready, *Effects of High Power Radiation*, Academic Press, New York, 1971.

21. W. W. Duley, *CO_2 Lasers: Effects and Applications*, Academic Press, New York, 1976.

22. R. Y. Chiao, E. Garmire, and C. H. Townes, "Raman and Phonon Masers," in *Quantum Electronics and Coherent Light*, Proc. Int. School. E. Fermi, edited by P. A. Miles, New York, 1964.

23. E. L. Kerr, "Filamentary Tracks Formed in Transparent Optical Glass by Laser Beam Self-Focusing. II. Theoretical Analysis," Phys. Rev. A, 4:1195 (1971).

24. C. W. Draper and S. L. Bernasek, "Directed Energy of Novel Metallic Surfaces," *NBS Special Publication 638*, p. 246, 1981.

25. A. L. Smirl, I. W. Boyd, T. F. Boggess, S. C. Moss, and H. M. van Driel, "Structural Changes Produced in Silicon by Intense 1-μm ps Pulses," J. Appl. Phys., **60**:1169 (1986).

26. S. M. Metev, S. K. Savtchenko, K. V. Stamenov, V. P. Veiko, G. A. Kotov, and G. D. Shandibina, "Thermochemical Action of Laser Radiation on Thin Metal Films," IEEE J. Quantum Electron., **QE-17**:2004 (1981).

27. A. E. Siegman and P. M. Fauchet, "Stimulated Wood's Anomalies on Laser-Illuminated Surfaces," IEEE J. of Quantum Electron., **QE-22**:1384 (1986).

28. M. R. Lange, J. K. McIver, and A. H. Guenther, "Laser Damage Threshold Predictions Based on the Effects of Thermal and Optical Properties Employing a Spherical Impurity Model," *NBS Special Publication 688*, p. 454, 1983.

29. A. F. Garito, K. D. Singer, C. C. Teng, "Molecular Optics: Nonlinear Optical Properties of Organic and Polymeric Crystals," in *Nonlinear Optical Properties of Organic and Polymeric Materials*, Washington, D.C.: ACS Symposium Series 233, ed. D. J. Williams, p. 18, 1983.

30. C. Flytzanis, "Optical Nonlinearities and Photoinduced Solitons in Conjugated Polymer Crystals," in *Nonlinear Optical Properties of Organic and Polymeric Crystals*, Washington, D.C.: ACS Symposium Series 233, ed. D. J. Williams, p. 169, 1983.

31. R. M. O'Connell and T. T. Saito, "Plastics for High-Power Laser Applications: A Review," Opt. Eng. 22:393 (1983).

32. R. M. O'Connell, T. F. Deaton, and T. T. Saito, "Single- and Multiple-Shot Laser Damage Properties of Commercial Grade PMMA," Appl. Opt. **23**:682 (1984).

33. A. V. Butenin and B. Ya. Kogan, "Mechanism of Transparent Polymer Material Damage Under Multiple Pulsed Laser Irradiation," Sov. J. Quantum Electron. **6**:611 (1976).

34. K. Dyumaev, A. A. Mamenkov, A. P. Maslyulov, G. A. Matyushin, V. S. Nechitailo, and A. S. Tsaprilov, "Transparent Polymers as a New Class of Optical Materials for Lasers," Sov. J. Quantum Electron. **12**:838 (1982).

35. J. H. Marburger, "Self-focusing: Theory," in *Progress in Quantum Electronics*, Vol. 4, edited by J. H. Sanders and S. Stenholm, Pergamon Press, New York, 1977.

36. W. E. Williams, M. J. Soileau, and E. W. Van Stryland, "The Effects of Self-Focusing on Laser-Induced Breakdown," Proc. 15th Annual Symp. on Opt. Mat. for High Power Lasers, Boulder, CO. 1983.

37. C. K. N. Patel, R. E. Slusher, and P. A. Fluery, "Optical Nonlinearities Due to Mobile Carriers in Semiconductors," Phys. Rev. Lett., **17**:1011 (1966).

38. F. Docchio, L. Dossi, C. A. Sacchi, "Q-Switched Nd:YAG Laser Irradiation of the Eye and Related Phenomena: An Experimental Study. III. Experimental Observation of Stimulated Brillouin Scattering in Eye Models," in *Lasers in Life Sciences*, New York: Harwood Academic Publishers, p. 117, 1986.

39. C. DeMichelis, "Laser Interaction with Solids—A Bibliographical Review," IEEE J. Quantum Electron., **QE-6**:630 (1970).

40. C. Kittel, *Introduction to Solid State Physics*, Wiley, New York, 1976.

41. J. P. Anthes, M. Bass, Appl. Phys. Lett., **31**:412 (1977).

42. D. C. Smith, "Laser Radiation-Induced Air Breakdown and Plasma Shielding," Opt. Eng., **20**:962 (1981).

43. S. Marcus, J. E. Lowder, D. L. Mooney, J. of Appl. Phys., **47**:2966 (1976).

44. M. Mohebi, G. Reali, M. J. Soileau, E. W. Van Stryland, "Self-Focusing in CS_2 at 10.6 μm," Opt. Lett., **10**:396 (1985).

45. J. B. Franck and M. J. Soileau, "A Technique for Increasing the Optical Strength of Single-Crystal NaCl and KCl Through Temperature Cycling," *NBS Special Publication 638*, pp. 114, 1981.

DISTRIBUTION
TECHNICAL REPORT # 0097

1 Commander
US Army Missile Command
ATTN: AMCPM-RD
Redstone Arsenal, AL 35809

1 Commander
MIRCOM
ATTN: DRSMI-FO
Redstone Arsenal, AL 35809

1 Commander
AVRADCOM
ATTN: DRCAV-BC
St. Louis, MO 63166

1 Commander
US Army Tank Automotive Command
ATTN: DRSTA-TSL
Warren, MI 48090

2 Commander
ESD/ACC
Hanscomb AFB, MA 01730

1 Commander
NARADCOM
ATTN: DRDNA-O
Natick, MA 01760

1 Commander
AMMRC
Watertown, MA 02172

1 Commander
HQ DARCOM
ATTN: DRCCP-E
Alexandria, VA 22333

2 Defense Technical Information Center
ATTN: DTIC-FDA
Cameron Station, Bldg 5
Alexandria, VA 22314-6145

3 Director
Defense Advanced Research Projects Agency
1400 Wilson Blvd.
Rosslyn, VA 22209

1 Commandant
Defense Systems Management College
ATTN: DRI-R
Fort Belvoir, VA 22060-5426

1 Commandant
US Army Engineer School
Fort Leonardwood, MO 65473-6650

Commander
Belvoir RD&E Center
2 ATTN: ASQNK-BVP-G
2 STRBE-BT (Tech Library)
Fort Belvoir, VA 22060-5606

CNVEO
1 ATTN: AMSEL-TMS/SEMCO
3 AMSEL-RD-NV-ISPD
1 AMSEL-RD-NV-D
20 AMSEL-RD-NV-LPD

Fort Belvoir, VA 22060-5677

1 Commander
USACSC
Fort Belvoir, VA 22060

1 Commander
US Operational Test and Evaluation Agency
ATTN: Tech Library
5600 Columbia Pike, Room 503
Falls Church, VA 22041

1 Director
Center for Signal Warfare
ATTN: AMSEL-RD-SW-D
Vint Hill Station, VA 22186

1 Commander
TRADOC
ATTN: ATCD-AN
Fort Monroe, VA 23651

1 Commander
US Naval Research Lab
Washington, DC 20375

1 HQDA
ATTN: DACA-CA
Washington, DC 20310

3 Commander
AFSC/ACC
Andrews AFB, MD 20334

1 Commander
US Army Systems Analysis Agency
Aberdeen Proving Ground, MD 21005

1 Commander
Harry Diamond Lab
ATTN: SLCHD-AC
Adelphi, MD 20783

1 Commander
US Naval Surface Weapons Center
White Oak
ATTN: Technical Library
Silver Spring, MD 20910

1 NASA Scientific & Tech Info Facility
ATTN: Acquisitions Branch (S-AK/DL)
Box 8757
BWI Airport, MD 21040

1 Director
CS&TA Laboratory
ATTN: DELCS-D
Fort Monmouth, NJ 07703

1 Director
Electronic Warfare Lab
ATTN: DELEW-D
Ft. Monmouth, NJ 07703

1 Director
Electronics Technology & Devices Lab
ATTN: DELET-D
Ft. Monmouth, NJ 07703

1 Commander
ARRADCOM
ATTN: DRDAR-SEC
Dover, NJ 07801

1 Commander
CORADCOM
ATTN: DRDCO-PPA-CA
Ft. Monmouth, NJ 07703

1 Commander
US Army Electronics R&D Command
ATTN: DELSD-L
Ft. Monmouth, NJ 07703-5301

3 Commander
US Army Communications and
Electronic Command
Ft. Monmouth, NYJ 07703-5007

1 Director
US Army Research and Technology Labs
Ames Research Center
Moffet Field, CA 94035

1 Commander
Naval Electronics Lab Ctr Library
San Diego, CA 92152

1 Director
Atmospheric Sciences
ATTN: DELAS-D
White Sands Missile Range, NM 88002

1 Armament Development and Test
ATTN: LOSL Tech Library
Elgin AFB, FL 32542